RSC Advances

This article can be cited before page numbers have been issued, to do this please use: V. Vrdoljak, G. Pavlovi, T. Hrenar, M. Rubi, P. Siega, R. Dreos and M. Cindric, *RSC Adv.*, 2015, DOI: 10.1039/C5RA22068H.

ROYAL SOCIETY OF CHEMISTRY

www.rsc.org/advances

View Article Online
ARTICLE TYPE www.rsc.org/xxxxxx DOI: 10.1039/b000000x | XXXXXXXX

Cobalt(III) complexes with tridentate hydrazone ligands: protonation state and hydrogen bonds competition

Višnja Vrdoljak,*[a] Gordana Pavlović,[b] Tomica Hrenar,[a] Mirta Rubčić,[a] Patrizia Siega,[c] Renata Dreos[c] and Marina Cindrić[a]

Received (in XXX, XXX) Xth XXXXXXXXX 200X, Accepted Xth XXXXXXXXX 200X
First published on the web Xth XXXXXXXXX 200X
DOI: 10.1039/b000000x

Cobalt(III) complexes of the type [Co(HL)(L)] were synthesized under solvothermal conditions staring from $[Co(C_5H_7O_2)_3]$ and the corresponding ligand H_2L (salicylaldehyde 4-hydroxybenzhydrazone, 3-methoxysalicylaldehyde 4-hydroxybenzhydrazone, 4-methoxysalicylaldehyde 4-hydroxybenzhydrazone, salicylaldehyde benzhydrazone, 3-methoxysalicylaldehyde benzhydrazone, 4-methoxysalicylaldehyde benzhydrazone). The presence of differently protonated forms of the same ligand in complexes was supported by IR and NMR spectroscopy as well as by the single crystal X-ray diffraction method. The effect of weak interactions on the supramolecular architecture and their role on the ligand form stabilization has been analysed. Molecular interactions within the unit cells were investigated and quantified by extensive quantum chemical analysis on models built from crystal structures using density functional theory and empirical dispersion. Ligands used in this study were prepared under environmentally friendly conditions by the mechanochemical synthesis. Their thermal behaviour and phase transitions were investigated using TG and DSC analysis and the powder X-ray diffraction method.

Introduction

The chemistry of hydrazones has been receiving an ongoing attention in various fields, ranging from organic synthesis[1–3] and medicinal chemistry[4–6] to supramolecular and coordination chemistry.[7–12] The hydrazone moiety can undergo reversible structural changes upon photochemical treatment and triggers like pH or temperature changes.[13–17] Different arrangements or conformations can lead to significant changes in physical and chemical properties of hydrazones and their complexes which make them attractive materials in connection with their potential applications.[18–22] Metal complexes with aroylhydrazone ligands ArC=N−NH−(C=O)−R are usually mononuclear or dinuclear. Some examples of structurally characterized complexes are $[Sn(L)(Ph)_2]\cdot EtOH$,[23] $[Cd(HL)_2]$,[24] $[Cu_2(L)_2(py)_2]$,[25] $[Cu_2(HL)_2(H_2O)_2](NO_3)_2$,[26] $[Co(HL)_2]ClO_4\cdot H_2O\cdot CH_3CN$,[27] $[Co(L)_2]_2[Co(H_2O)_4(OPPh_3)_2]$,[28] $[Co(L)_2]Cl$,[29] $[Co(L)_2]\cdot H_2O$,[30] or $[Co(L)(HL)_2](NO_3)_2\cdot H_2O\cdot CH_3OH$.[31] In these compounds, the hydrazone ligand is in the singly-deprotonated HL^-, or in doubly-deprotonated L^{2-} form, Scheme 1. The protonation state of these ligands in metal complexes plays an important role since it offers fine-tuning of properties such as electrochemical, photophysical or catalytic.[32–34]

Although numerous transition metal complexes with aroylhydrazone derivatives are known, related cobalt(III) complexes are rare. Only seven such structures have been published to date.[27–39] In addition, complexes based on differently deprotonated ligand are even more scarce. The structures of the complexes [Fe{H(3,5-^{t}Bu$_2$)salbh}{(3,5-^{t}Bu$_2$)salbh}],[40] and [Fe(L)(HL)],[41] containing the 3,5-di-*tert*-butylsalicylidene benzoylhydrazine, or *N*-(2-oxo-3-methoxybenzilidene)-benzohydrazide, respectively, represent such examples.

Inspired by the previously mentioned facts in this work we were interested to investigate mononuclear cobalt(III) complexes which bear tridentate ONO hydrazone ligands in different protonation states. Such complexes can be formulated as [Co(HL)(L)], where HL denotes singly deprotonated ligand and L doubly deprotoneted one. In this comprehensive study we employed X-ray crystallography, IR and NMR spectroscopy as well as quantum chemical calculations to analyze: (i) structural and electronic changes of the hydrazone moiety depending on the protonation state of ligand; (ii) importance of nonbonding interactions in the stabilization of particular ligand form and (iii) potential role of N–H···O/N or O–H···O/N hydrogen bonds in the overall stabilization of the crystal structure.

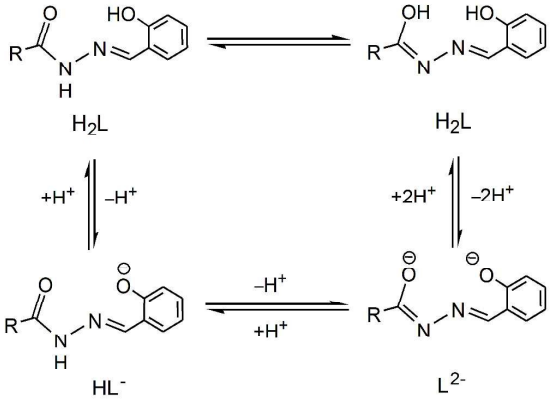

Scheme 1 Tautomerism of hydrazone ligand and reversible deprotonation

View Article Online
DOI: 10.1039/C5RA22068H

As a part of this study we also aimed to investigate synthesis of aroylhydrazone ligands under more environmentally friendly conditions. For this purpose we employed mechanochemical synthesis which has been extensively investigated lately as a "green" synthetic route.[42,43] It has been applied to various organic reactions, including condensation reactions, nucleophilic additions, Diels–Alder reactions, *etc.*[44] The first synthesis of hydrazones using ball-milling method was reported by Kaupp and coworkers.[45,46] Baltas *et al.* recently reported solvent-free mechanochemical route for pharmaceutically attractive phenol hydrazones using a vibratory ball mill with an average reaction time of four hours.[47]

Results and Discussion

Synthesis of hydrazone ligands

Synthesis of ligands was carried out using equimolar amounts of the corresponding aldehyde (salicylaldehyde, 3-methoxysalicylaldehyde or 4-methoxysalicylaldehyde) and hydrazide (4-hydroxybenzhydrazide or benzhydrazide) under mechanochemical conditions, Scheme 2. Reactions were performed by liquid-assisted grinding of the reagents in presence of a small amount of methanol and acetanhydride. The powder X-ray diffraction (PXRD) revealed the complete disappearance of reflections corresponding to starting compounds after 20–60 min (Table 1). It should be noted that the addition of acetanhydride/methanol mixture led to a significant reduction of the reaction time comparing to the results obtained when catalyst was not added to the reaction mixture.

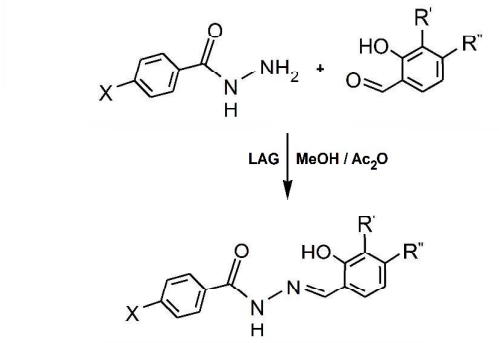

	R'	R''	
X = OH	H	H	H_2L^1
	OCH_3	H	H_2L^2
	H	OCH_3	H_2L^3
X = H	H	H	H_2L^4
	OCH_3	H	H_2L^5
	H	OCH_3	H_2L^6

Scheme 2 Synthesis of hydrazone ligands $H_2L^{1\text{-}6}$.

Table 1 Synthesis of hydrazone ligands.

Ligand	Aldehyde[a]	Hydrazide[b]	Milling time/min
H_2L^1	Sal	HBOH	40
$H_2L^2{\cdot}H_2O$	3-OMe-Sal	HBOH	20
$H_2L^3{\cdot}H_2O$	4-OMe-Sal	HBOH	60
H_2L^4	Sal	HB	30
$H_2L^5{\cdot}H_2O$	3-OMe-Sal	HB	30
$H_2L^6{\cdot}H_2O$	4-OMe-Sal	HB	60

[a] Sal (slicylaldehyde), 3-OMe-Sal (3-methoxysalicylaldehyde), 4-OMe-Sal (4–methoxysalicylaldehyde); [b] HBOH (4-hydroxybenzhydrazide), HB (benzhydrazide)

Compounds H_2L^1 and H_2L^4 were found to be unsolvated, whereas $H_2L^2{\cdot}H_2O$, $H_2L^3{\cdot}H_2O$, $H_2L^5{\cdot}H_2O$ and $H_2L^6{\cdot}H_2O$ were obtained in their hydrated forms. They were analyzed by PXRD (Fig. 1) thermogravimetric (TG) and differential scanning calorimetric measurements (DSC, see ESI Figs. S1−S6†). PXRD patterns for prepared hydrazones were compared to those calculated from the previously reported single crystal X-ray crystallography studies, Fig. 1 ((a) H_2L^1, CSD code YIFPAF01;[48] (b) $H_2L^2{\cdot}H_2O$, CSD code ROGFEZ;[49] (c) $H_2L^3{\cdot}H_2O$, CSD code MOKRUA;[50] (d) H_2L^4, CSD code ZAYQAR;[51] (e) $H_2L^5{\cdot}H_2O$, CSD code TEZMER[52] and (f) $H_2L^6{\cdot}H_2O$, CSD code MIQXUH).[53] The appearance of experimental diffraction patterns is consistent with those simulated for all compounds.

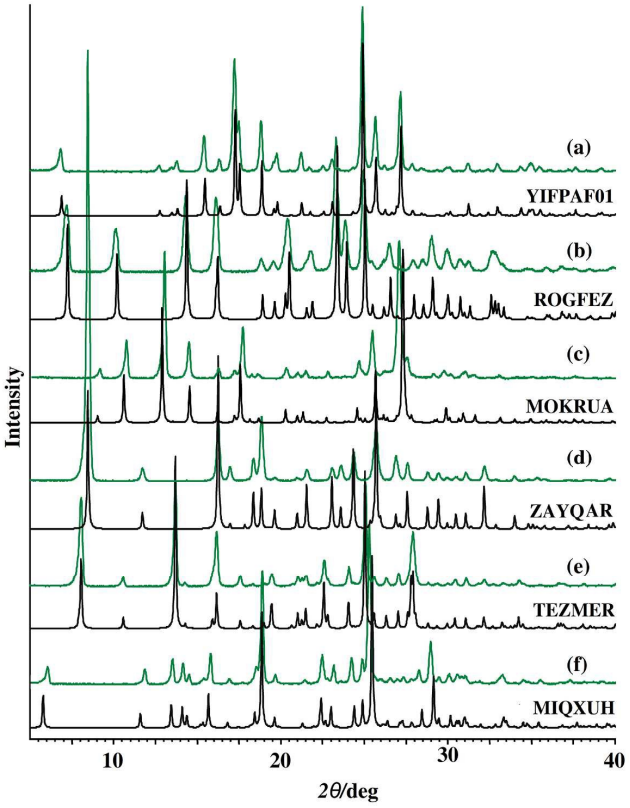

Fig. 1 Comparison of the PXRD patterns for mechanochemically prepared ligands (the green lines: (a) H_2L^1; (b) $H_2L^2{\cdot}H_2O$; (c) $H_2L^3{\cdot}H_2O$; (d) H_2L^4; (e) $H_2L^5{\cdot}H_2O$ and (f) $H_2L^6{\cdot}H_2O$), and calculated from the deposited crystal structure (the black lines with CSD code).

View Article Online
DOI: 10.1039/C5RA22068H

Their thermal behaviour and phase transitions were investigated using TG and DSC analysis and the powder X-ray diffraction method. The first mass loss in the TG curves of $H_2L^2{\cdot}H_2O$, $H_2L^3{\cdot}H_2O$, $H_2L^5{\cdot}H_2O$ and $H_2L^6{\cdot}H_2O$ was related to the water molecule release (6.1%, 5.0%, 6.7% and 6.0%, respectively). The dehydration process was observed as a broad endothermic peak in DSC thermograms. Afterward, an exothermic peak appeared in thermograms of H_2L^3 and H_2L^5 (Figs. S3 and S5) suggesting a solid-to-solid phase transformation (see ESI Figs. S7 and S8†). On the other hand, in the case of $H_2L^2{\cdot}H_2O$ and $H_2L^6{\cdot}H_2O$ an exothermic peak during the heating process was not observed (Figs. S2 and S6†). To inspect in detail, samples were heated from the ambient temperature at various heating rates (2, 10, 20 and 50 °C min^{-1}). Again, no peaks were observed up to the temperature associated with melting endotherm. As seen form PXRD patterns the absence of the solvent molecule in H_2L^2 induced certain shifts in the peak position whereas in case of H_2L^6 the unsolvated compound showed a diffractogram significantly different from that of $H_2L^6{\cdot}H_2O$ (see ESI Figs. S9 and S10†). Additionally, the resulting materials obtained by the solid state desolvation of $H_2L^5{\cdot}H_2O$ and $H_2L^6{\cdot}H_2O$ exhibited PXRD patterns consistent with those simulated from the single-crystal data for the anhydrous H_2L^5 and H_2L^6, respectively (Fig. S8 and S10).

The melting endotherms of the anhydrous hydrazones are very sharp, occurring over a narrow temperature interval thus indicating purity of the compounds. From DSC measurements it follows that the melting points for H_2L^{1-6} were 268 °C ($\Delta_{fus}H$ = 37 kJ mol^{-1}), 194 °C ($\Delta_{fus}H$ = 25 kJ mol^{-1}), 229 °C ($\Delta_{fus}H$ = 31 kJ mol^{-1}), 179 °C ($\Delta_{fus}H$ = 22 kJ mol^{-1}), 191°C ($\Delta_{fus}H$ = 32 kJ mol^{-1}) and 181 °C ($\Delta_{fus}H$ = 25 kJ mol^{-1}), respectively.

Synthesis of cobalt(III) complexes with hydrazone ligands

The mononuclear cobalt(III) complexes $[Co(HL^{1-6})(L^{1-6})]$ (**1–3**) were prepared solvothermally in methanol by the reaction of $[Co(acac)_3]$ with the corresponding hydrazone ligand H_2L^{1-6} in a 1:2 metal to ligand ratio. Reactions were also performed in methanol under refluxing conditions. However, they resulted in a significantly lower yield even after longer reaction time. All complexes are dark red crystalline solids soluble in coordinating solvents such as dmf or dmso and only moderately soluble in pyridine, picoline or methanol. Thermal stability of these complexes was investigated in the atmosphere of pure oxygen. The first step in the thermogravimetric curve of **6·MeOH** was related to the loss of MeOH molecule (131–155 °C) and was followed, on further heating, by significant weight loss at 291 °C due to ligand decomposition. For TG measurement, the crystals of **2·0.7MeOH** were stored into a desiccator and then placed in a freezer (at −15 °C). TG measurement showed gradual mass loss in the range 159–285 °C ascribed to loss of methanol (see ESI Fig. S11(a)†). Desolvation of **2·0.7MeOH** also occurred upon prolonged standing at room temperature and afforded the stable crystalline form of **2** as the final residue (Fig. S11(b)). Compounds **1–6** started to decompose at 317 °C for **1**, 330°C for **2**, 331 °C for **3**, 347 °C for **4**, 297 °C for **5**, 291 °C for **6**.

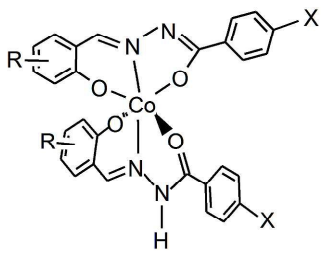

Scheme 3. The structural formula of [Co(HL)(L)] complex (showing hydrazonato HL^- form and hydrazidato L^{2-} form).

In all compounds formed after chelation, the ligands were found to exist in differently deprotonated forms (Scheme 3). The protonation state and formation of [Co(HL)(L)] was supported by IR and NMR spectroscopy as well as by the single crystal X-ray diffraction method.

Molecular and crystal structures of the H_2L^3, H_2L^5 and H_2L^6 ligands

Crystals of the anhydrous hydrazones H_2L^3, H_2L^5 and H_2L^6 suitable for single crystal X-ray diffraction (SCXRD) were obtained from ethanol.[54] In the crystal structures of all three ligands, hydrazone molecules are found in the same tautomeric form. As it is evident from the relevant bond distances (see ESI, Table S1†),[55] aldehyde residues of the molecules adopt the enol-imino form, while their hydrazone −(C=O)− linkages assume the keto form. In each case, the molecular structure is stabilized by a strong intramolecular hydrogen bond of the O–H···N type, characteristic for the *o*-hydroxy Schiff bases (Table S1).

H_2L^3 molecules adopt a *syn*-configuration, when taking into consideration relative position of O1 and O2 oxygen atoms (Fig. 2 a)). The 4-methoxysalicylidene residue and the central hydrazone linkage, =N−NH−(C=O)−, are essentially coplanar, while the terminal 4-hydroxybenzene ring is twisted in such a way to form a dihedral angle of 39.94(6)° with respect to the plane of the aldehyde ring. Crystal structure of H_2L^3 unveils a complex hydrogen bonding network formed by two types of intersecting hydrogen-bonded chains (see ESI, Fig. S12†). The first type corresponds to infinite *zig-zag* hydrogen-bonded *C*(8) chains that grow parallel to *b*-axis and are realized through O3–H3O···O1 hydrogen bonds. As each molecule additionally associates with the neighbouring ones *via* N2–H2N···O2 hydrogen bonds, it leads to formation of the second type of hydrogen-bonded chain, *C*(7) one, which runs along the *c*-axis. Supramolecular assembly formed in such a way is further stabilized and extended into a three-dimensional network through C–H···O interactions (Fig. S12).

View Article Online
DOI: 10.1039/C5RA22068H

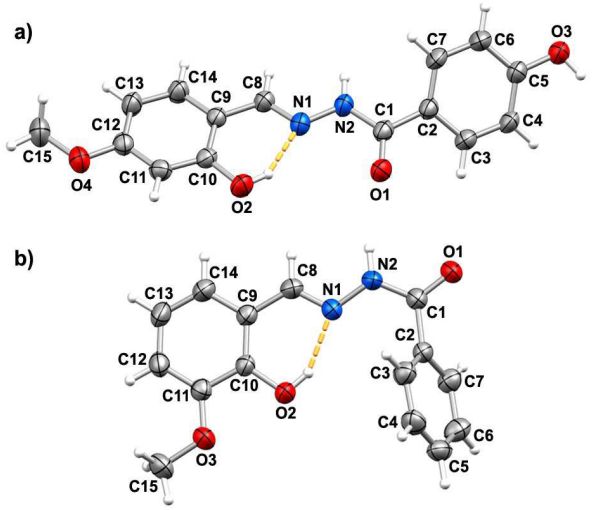

Fig. 2. Mercury-rendered ORTEP view of molecular structures of: a) H_2L^3, and b) H_2L^5. The displacement ellipsoids are drawn at the 50% probability level at 296(2) K while the hydrogen atoms are drawn as spheres of arbitrary radius. Intramolecular hydrogen bonds of the O–H···N type, yielding a *S*(6) motif, are shown as orange dashed line.

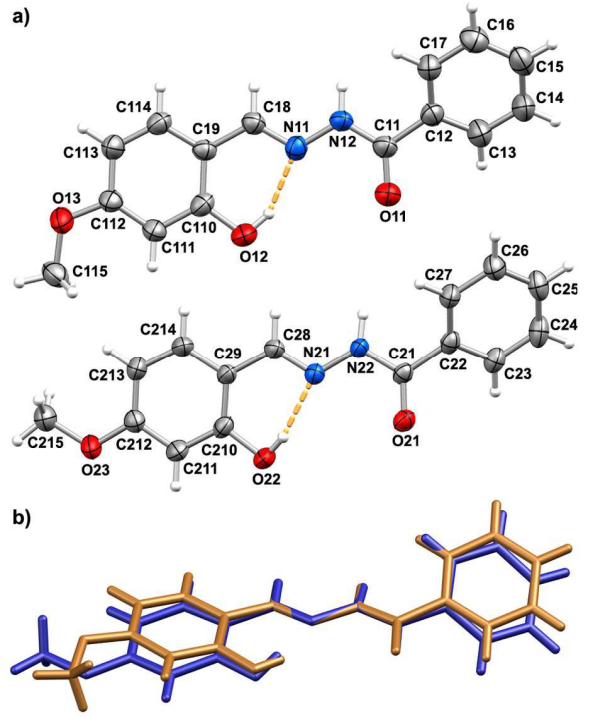

Fig. 3. a) Mercury-rendered ORTEP view of molecular structures of the two molecules constituting the asymmetric unit of H_2L^6 (top-molecule 1; bottom-molecule 2). For clarity, molecules are not shown in their true position within the asymmetric unit. The displacement ellipsoids are drawn at the 30% probability level at 296(2) K. The hydrogen atoms are drawn as spheres of arbitrary radius. Intramolecular hydrogen bonds of the O–H···N type are shown as orange dashed lines. b) Overlapping diagram of the two molecules comprising the asymmetric unit of H_2L^6 (light brown-molecule 1; blue-molecule 2). The diagram was constructed by overlying O11, C11, N12 and N11 atoms with O21, C21, N22 and N21 atoms, respectively. Dihedral angle between the planes of the aldehyde and the benzene rings is 26.9(3)° for molecule 1, and 35.5(3)° for molecule 2.

As opposed to molecules of H_2L^3, those of H_2L^5 assume an *anti*-configuration when considering the position of O1 and O2 atoms (Fig. 2 b)). While the inner hydrazone portion and the aldehyde part of the molecule remain planar, the terminal benzene ring is tilted 62.30(8)° away from this plane. The adopted *anti*-configuration with favourable alignment of hydrogen bond donors and acceptors allows formation of centrosymmetric hydrogen-bonded dimers, displaying a $R_2^2(8)$ motif which is accomplished through N2–H2N···O1 hydrogen bonds (see ESI, Fig. S13†). The dimers associate *via* C7–H7···O2 interactions into endless chains which run along the *b*-axis. Such chains are joined into layers *via* C5–H5···O3 interactions, which are finally stacked through van der Waals interactions (Fig. S13).

4-methoxysalicylaldehyde benzhydrazone (H_2L^6) crystallizes in the space group *Pc* with two molecules per asymmetric unit. As can be seen from Fig. 3 the two molecules differ substantially in the orientation of the methoxy moiety on the position four of the salicylaldehyde ring. Moreover, there is an apparent difference in the conformation of the molecules (Fig. 3), while both of them adopt a *syn*-configuration when referring to O1 and O2 atoms. In the crystal, molecules connect *via* N–H···O hydrogen bonds, each independent molecule with its own kind, thus forming hydrogen-bonded chains *C*(4) motifs which spread along the *c*-axis. Such chains are stabilized and mutually connected through C–H···O interactions (see ESI, Fig. S14†).

Molecular and crystal structure of 2

The asymmetric unit of **2** contains complex molecule in general crystallographic position and loosely bound 0.7 methanol of crystallization per complex molecule (Fig. 4). The methanol molecules are arranged within channels of the crystal structure along the *a* axis (Fig. S15, see ESI†). The Co(III) ion is octahedrally coordinated *via* two ONO tridentate ligands which differ in their protonation state, see Scheme 3) preserving electroneutrality of the complex molecule as a whole. The imino nitrogen atoms are axially positioned (Co1−N11 1.880(2) Å and Co1−N21 1.867(2) Å) and four oxygen atoms constitute equatorial plane of the octahedron. The deformation from ideal octahedral geometry is manifested in *trans* octahedral bond angles values which amount 171.65(10)°, 177.53(9)° and 178.75(9)° and *cis* octahedral bond angles values which are in the range 83.18(10)° − 94.87(10)°.

The Co−O(phenolate) bonds values amount 1.879(2) Å and 1.899(2) Å for Co1−O12 and Co1−O22 bonds, respectively, and the Co−O cobalt-to-(hydrazonato) oxygen atoms bond distance values amount: Co1−O11 1.928(2) Å and Co1−O21 1.884(2) Å. One ligand acts in a hydrazonato HL^- form, while the other is in the hydrazidato L^{2-} form (at O12 in the first ligand, and O22 and O21 in the second one). Since the ligand molecule labelled as first one is in the singly-deprotonated form, the trend that Co1−O11 bond distance (1.928(2) Å) is longer than Co1−O12 bond distance (1.879(2) Å) in the same ligand is expected.

View Article Online
DOI: 10.1039/C5RA22068H

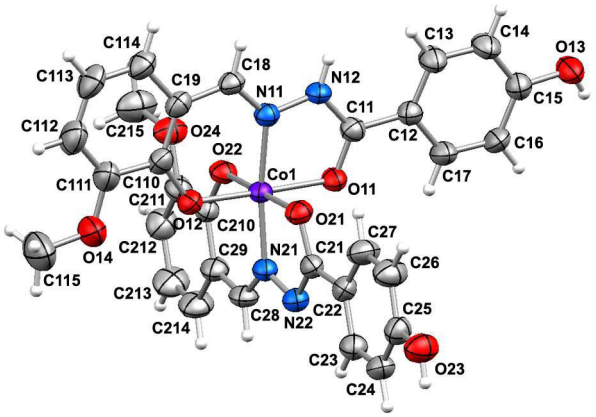

Fig. 4. Mercury–rendered ORTEP view of the molecular structure of complex **2·0.7MeOH**. The displacement ellipsoids are drawn at the 50% probability level at 296(2) K after use of SHELXL-2013 SQUEEZE instruction. The atom-numbering crystallographic scheme has been applied. The hydrogen atoms are drawn as spheres of arbitrary radius.

On the other hand, comparing bond distances within the coordination sphere, the O21 atom of the doubly deprotonated ligand (Co1−O21 bond distance of 1.884(2) Å within the five-membered chelate ring fragment) is found to be more tightly bound to the Co(III) ion than the O11 atom of the singly-deprotonated ligand (Co1−O11 1.928(2) Å). The similar trend one can observe for Co1−N11 1.880(2) Å and Co1−N21 1.867(2) Å bonds exhibiting stronger bond with the nitrogen atom of the doubly-deprotonated hydrazonato ligand enhanced by more pronounced delocalization.

The coexistence of both forms within a complex is evidenced by the bond distances values (see ESI Table S3a†) in the region of five-membered chelate ring which is in agreement with the position of the electron density maximum corresponding to the H12N hydrogen atom of the hydrazone NH group. Therefore, the keto C11−O11 bond distance values amounts 1.278(3) Å, on the contrary to the value of 1.309(3) Å for the O21−C21 bond distance value. The N12−C11 bond distance of 1.333(4) Å is more σ in character opposite from N22−C21 which is shortened to the value of 1.315(4) Å.

The proton of the hydroxyl O23−H23O is bifurcated between two proton acceptors; one is phenolate oxygen O12 atom and the other is methoxy O14 atom, Fig. 5. The supramolecular centrosymmetrical ring is formed *via* O23−H23O···O12 intermolecular hydrogen bond between hydroxyl group and phenolate O12 donor atom (see ESI Fig. S16, Table S4†). The O13−H13O···N22 intermolecular hydrogen bond of 2.734(4) Å between hydroxyl O13−H13O group and the non-donor nitrogen atom N22 forms another supramolecular hydrogen bonded ring which alternates within crystal structure of **2** with the former (Fig. 5, Table S4†). Bifurcation of the N12−H12N proton-donor group in **2** between two proton acceptors: the phenolate O22 atom and the methoxy O24 atom are shown in Fig. 6. Therefore, two intermolecular hydrogen bonds are formed: N12−H12N···O22 and N12−H12N···O24 (Table S4†). The formation of 3D hydrogen bonded network including all above mentioned types of hydrogen bonds is given in ESI, Fig. S17.

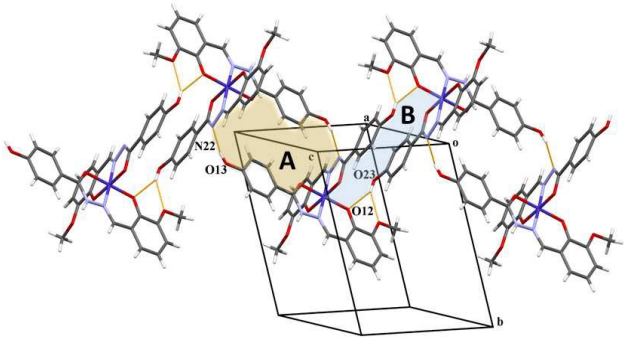

Fig. 5. The alternated assembling of two supramolecular hydrogen bonded rings *via* O13−H13O···N22 (ring A) and O23−H23O···O12 (ring B) intermolecular hydrogen bonds in the crystal structure of **2**.

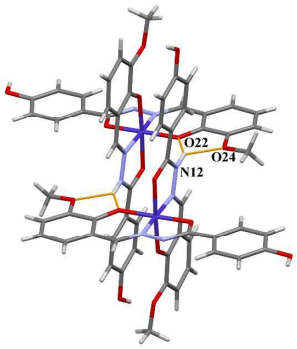

Fig. 6. Bifurcation of N12−H12N group at two proton donors in **2** between two proton acceptors: the phenolate O22 atom and the methoxy O24 atom thus forming two hydrogen bonds: N12−H12N···O22 of the distance value 3.066(3) Å and N12−H12N···O24 2.770(4) Å.

Molecular and crystal structure of 1 and 6·MeOH

The Co(III) ion in **1** and **6·MeOH** is situated at crystallographically imposed two-fold axis (Fig. S18, Fig. S19, see ESI†). In this way, the asymmetric unit contains half of the complex molecule. The coordination around Co(III) ion in both complexes is best described as a distorted octahedron formed by two condensed chelate rings comprising tridentate ONO aroylhydrazone ligands. From the crystallographical point of view, both ligands are represented as an average of hydrazonato HL^- and hydrazidato L^{2-} forms, which is achieved by occupational factor of H12N atom to be set up as 0.5 during crystallographic refinement. Therefore, the request for symmetry and simultaneously for complex electroneutrality is preserved.

In complex **1** each of the two ligands coordinate to Co(III) ion with the hydrazone oxygen (Co1−O1 1.892(2) Å), phenolate oxygen (Co1−O2 1.884(2) Å) and imine nitrogen donor atoms (Co1−N1 1.874(3) Å) being in axial positions, to form two chelate rings: six-membered with the O2 and N1 donor atoms and five-membered with the N1 and O1 donor atoms. The deformation from ideal octahedral geometry is manifested in *trans* octahedral bond angles values which amount 172.05(18) and 178.70(10)° and *cis* octahedral bond angles values which are in the range 83.68(11)° − 95.24(11)° (Table S3(b)).

The structurally analogous complex **6** exhibits comparable geometrical parameters: (Co1−O1 1.921(2) Å, Co1−O2

View Article Online
DOI: 10.1039/C5RA22068H

1.886(2) Å and Co1−N1 1.876(2) Å) (Table S3(b)). In the region of five-membered chelate ring, which is most dependent on the type of forms, HL^- or L^{2-}, the C1−O1 bond distance of 1.289(4) and 1.285(3) Å in **1** and **6·MeOH**, respectively, and N2−C1 bond distance of 1.325(4) and 1.331(4) Å in **1** and **6·MeOH**, respectively, are an average of the HL^- and L^{2-} five-membered chelate rings (Table S3b).

In complex **1** the co-existence of two ligand forms, which differ in their protonation states, is maintained by the intermolecular hydrogen bond N2−H12N···N2 (Table S4). The hydrogen bond distance value of 2.811(4) Å and bond angle value of 163(7)° (for the N2−H12N···N2 angle) are both within expected range values for N−H···N type of hydrogen bond. This hydrogen bond assembles complex molecules into infinite 1D chain along *a* axis (Fig. 7).

The H13O hydrogen atom of the hydroxyl group of 4-hydroxybenzhydrazone ligand is bifurcated thus forming two intermolecular hydrogen bonds with the phenolate O2 and imine N1 atoms (Table S4†) with the former bond being expectedly stronger and more linear. The O3–H13O···O2 intermolecular hydrogen bonds forms infinite 2D chains of fused rings spreading along *b* axis in a *zig-zag* manner (see ESI; Fig. S20†).

The crystal structure of **6·MeOH** is dominated by the N−H···O type of intermolecular hydrogen bond (Table S4). The other hydrogen bonds are of the C–H···O type and include all oxygen atoms O1, O2, O3 and O4 (see ESI; Fig. S21†).

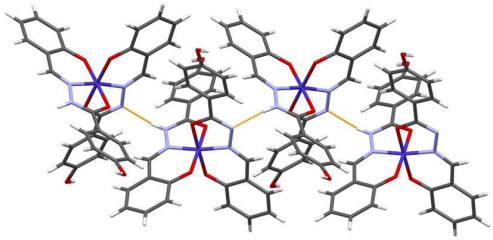

Fig. 7. Fraction of crystal structure of complex **1** showing assembling of complex molecules in *ac* plane into 1D infinite chains *via* N2–H12N···N2 intermolecular hydrogen bond (denoted as orange dashed line).

Quantum chemical calculations

In order to investigate and quantify molecular interactions within the unit cells, extensive quantum chemical analysis was performed. Firstly, models of four complexes of **1** and four complexes of **2** were built from crystal structures and geometry optimization were performed using B3LYP hybrid functional and D3 version of Grimme's dispersion with Becke-Johnson damping[56] with 6-31g(d) basis set (Figs. 8a and 9a). After that the model **1'** of four complexes of **1** with the same packing of structure **2** was built by removing methoxy groups from ligands in the optimized structure of **2** (Figs. 8b). *Vice versa*, the model **2'** of four complexes of **2** with the same packing of structure **1** was built by adding methoxy groups on the optimized structure of **1** (Fig. 9b). Additional geometry optimizations and harmonic frequency calculations were performed. The goal of this analysis was to establish the quantitative relationship between the structures by comparing standard Gibbs energies of formation and checking the dominant molecular interactions in crystal structures of **1** and **2**.

According to the calculated values (Table 2) crystal structures of **1** and **2** were more stable than **1'** and **2'**, respectively. The presence O–H···O and N–H···N hydrogen bonds in **1** was shown to be a stability factor in contrast to O–H···N and N–H···O hydrogen bonds in **1'** (Fig. 8). Likewise, the presence of O–H···N hydrogen bond and bifurcated hydrogen bond between N–H group of singly-deprotonated ligand and phenolate and methoxy oxygen atoms in **2** was shown to be more stable than N–H···N hydrogen bond and bifurcated hydrogen bond between the O–H group and phenolate and methoxy oxygen atoms in **2'**, respectively (Fig. 9, Table 2).

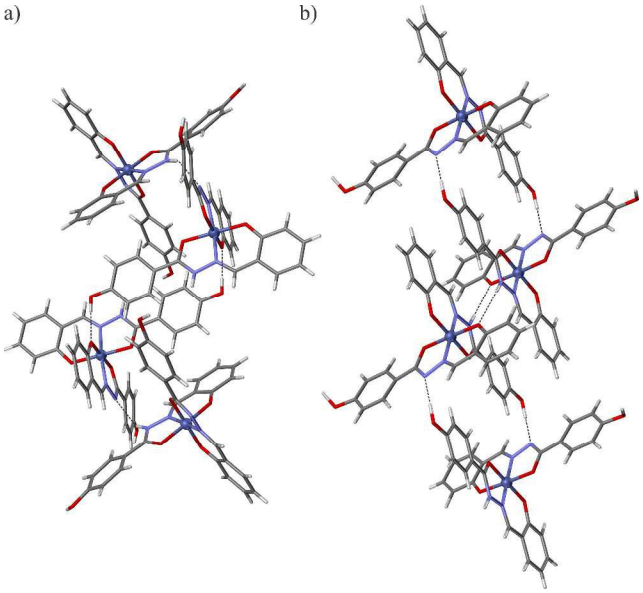

Fig. 8. Tetrameric model of a) crystal structure of **1** and b) **1'** (**1** with the same packing as in **2**).

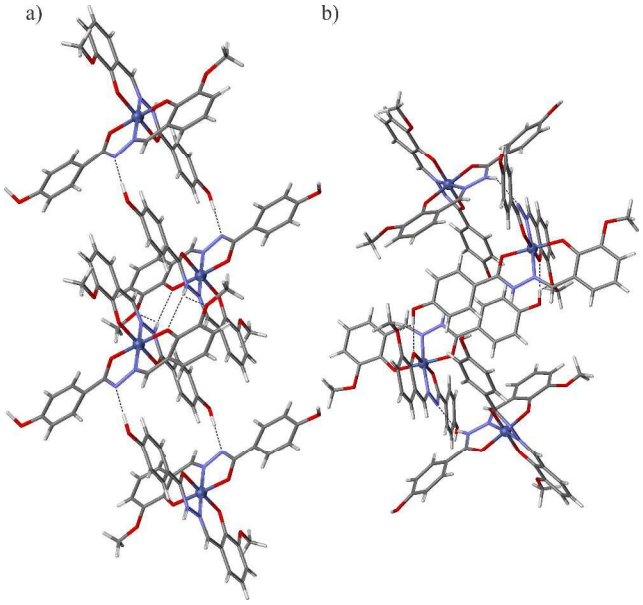

Fig. 9. Tetrameric model of a) crystal structure of **2** and b) **2'** (**2** with the same packing as in **1**).

View Article Online
DOI: 10.1039/C5RA22068H

Table 2. Standard Gibbs energies of formation for four complexes of **1** and **2** and models **1'** and **2'** build from their crystal structures calculated with B3LYP and D3 version of Grimme's dispersion with Becke-Johnson damping with 6-31g(d) basis set.

Compound	$\Delta_f G°$/kJ mol^{-1} (relative to **1**)	$\Delta_f G°$/kJ mol^{-1} (relative to **2**)
1 (built from crystal structure)	0.0	–
1' (built from crystal structure of **2**)	190.41	–
2 (built from crystal structure)	–	0.0
2' (built from crystal structure of **1**)	–	145.82

Comparative structural analysis

The molecular structures of **1** and **6·MeOH** exhibit metrical parameters resemblance. Namely, both complexes contain Co(III) ion positioned at two-fold axis and thus both forms, singly- and doubly-deprotonated form of the particular ligand, are present as an averaged structure preserving electroneutrality of the complex molecule as a whole. On the contrary, the asymmetric unit of **2** reveals Co(III) ion coordinated by HL^- and L^{2-} ligand forms, separately. This is crystalographically evidenced as the averaged metrics of two different ligand forms in **1** and **6·MeOH** in comparison with two ligand forms in **2** (Table 3).

Table 3. Comparison of bond distances within five-membered chelate ring (Å) in **1**, **2** and **6·MeOH**

Bond	**1**	**6·MeOH**	HL^- ligand in **2**	L^{2-} ligand in **2**
N1−N2	1.403(4)	1.405(3)	N11−N12 1.380(3)	N21−N22 1.385(4)
N2−C1	1.325(4)	1.331(4)	N12−C11 1.333(4)	N22−C21 1.315(4)
C1−O1	1.289(4)	1.285(3)	O11−C11 1.278(3)	O21−C21 1.309(3)

Although, ligand skeleton is highly delocalized π system (particularly that which is doubly-deprotonated), it is apparent that O11−C11 bond distance in **2** reflects dominantly double character, while O21−C21 in **2** is dominantly σ in character. As opposed, the C1−O1 bond distances in **1** and **6·MeOH** are intermediates between a carboxyl C−O single (1.31 Å) and C=O double bond (1.21 Å). The shortest C=N bond distance value is expectedly found in the doubly-deprotonated form (N22-C21 1.315(4) Å in **2**), while the analogous bond distance in the singly-deprotonated form (N12−C11 1.333(4) Å in **2**) is in accordance with its more pronounced single-bond character.

The presence of both ligand forms HL^- and L^{2-} in **1** and **6**·MeOH is stabilized *via* supramolecular assembling by means of the N2−H12N···N2 intermolecular hydrogen bond in **1** or N2−H12N···O4 in **6·MeOH** with MeOH molecule. In both cases, 1D infinite chains are formed resulting in channels that spread in each space dimension of the crystal structure (Fig. 10).

This stabilization occurs in **2** in the way that the proton donor N12−H12N group of HL^- ligand forms hydrogen bonded centrosymmetrical dimers with the methoxy oxygen atom of the adjacent complex molecule showing bifurcation by forming additional hydrogen bond with the phenolate oxygen atom. This additional bond is responsible for the interconnected structure with smaller number of channels (Fig. 11). The channels that are formed in the structure of **2** are suitable for accommodation of the methanol molecules (Fig. S15†).

Although, both complexes **2** and **6·MeOH** contain $–OCH_3$ group; in complex **6·MeOH** it acts as proton acceptor in the formation of the C–H···O type of the hydrogen bond, and not in the formation of hydrogen bond with –NH group, like in **2**. Thus, the supramolecular role of MeOH solvent molecule of crystallization in the stabilization of hydrogen bonding is evident considering its competition with $–OCH_3$ group for hydrogen bond formation with the –NH group.

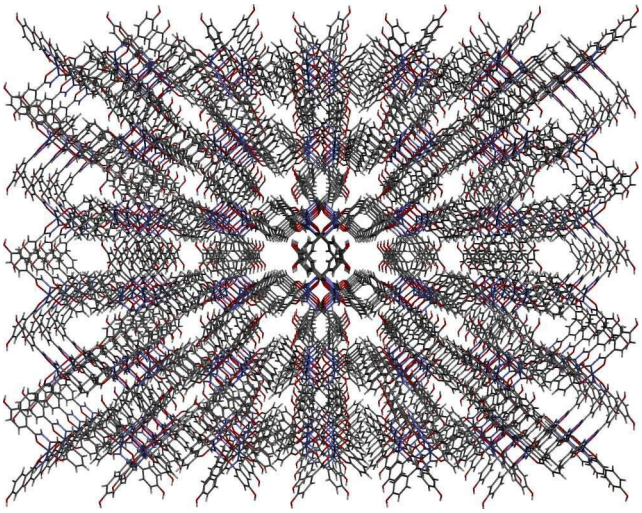

Fig. 10. Channels in the structure of **1** spreading in *a*-axis direction (similar is in *b*- and *c*-axis directions).

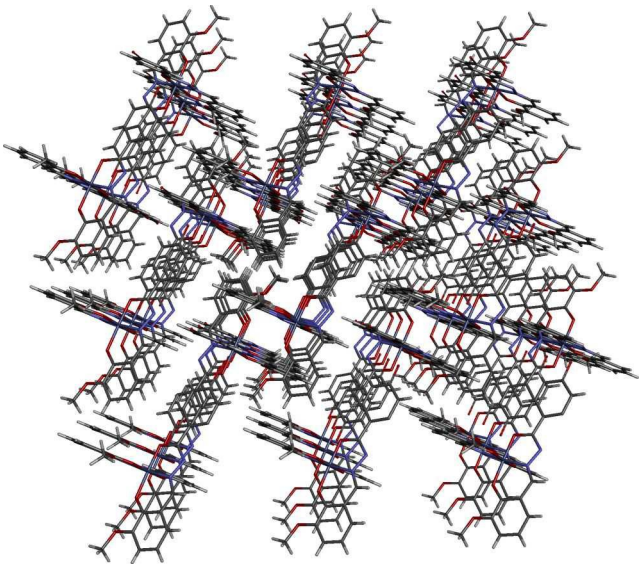

Fig. 11. Channels in the structure of **2** spreading in *c*-axis direction (there are no similar channels in other directions).

View Article Online
DOI: 10.1039/C5RA22068H

NMR spectroscopy

Complexes **1**−**6** were characterized *via* 1D and 2D ^{1}H NMR spectroscopy in DMSO-d_6 (see ESI, Fig. S22-S27). The ^{1}H NMR spectra of all the complexes, recorded immediately after dissolution, show only one set of signals, in agreement with a centrosymmetric configuration of the complexes. The signals due to the C10-OH and to =N−NH are absent in the spectra of the coordinated chelates, indicating that the ligands undergo deprotonation and that the protons involved in the intermolecular hydrogen bonds exchange fast in solution. The N=CH resonance is shifted downfield of about 0.3 ppm relative to the free ligand, as a result of the electronic redistribution consequent to complexation, as it was previously observed for the related Mo complexes.[57] These data indicate that the coordination mode found in the crystal structures is retained in solution. The signals of the C5-OH protons in complexes **1**−**3** are broad and they are likely involved in a chemical exchange process.

The ^{1}H NMR spectra of **1** and **4** did not change with time. On the contrary, a second set of signals, corresponding to the free ligand, developed in the spectra of the other complexes. This second set increased with time, reaching after about 10 days an integrated intensity, relative to the signals of the starting complexes, of 3% and 6% for **2** and **5**, respectively, and of 7% and 23% for **3** and **6**. The above results suggest a different stability of the complexes in DMSO-d_6 solution, the complexes with the $H_2L^{1,4}$ ligands being more stable than those with $H_2L^{2,5}$ and those with $H_2L^{3,6}$ being the least stable.

In order to investigate the acid-base behaviour of the complexes in solution, a ^{1}H NMR titration was carried out on **1** and **5**. The complexes dissolved in DMSO-d_6 (about 5×10^{-3} mmol in 0.8 mL of solvent) were titrated in the NMR tube with a 0.5 M solution of NaOH dissolved in D_2O. The chemical shift changes relative to the starting complex ($\Delta\delta$) were plotted at different [NaOH]/[complex] ratios. For **5**, all the resonances are shifted upfield up to the addition of about a 1:1 amount of NaOH (see ESI, Fig. S28(a)†), whereas successive additions do not cause a further shift, indicating that the complex behaves as a monoprotic acid. A parallel experiment carried out on **1** (see ESI, Fig. S28(b)†) shows a similar behavior for additions up to 1:1, but the signals keep moving upfield for further additions of NaOH (up to about a 3:1 ratio). This second acid-base process affects mainly the resonances of the protons closer to C5-OH, indicating that the deprotonation occurs at the phenolic protons.

It is worth of noting that, for [NaOH]/[complex] ratios ranging from about 1 to about 3, the upfield shift is associated with a severe broadening of the signals at 6.75 ppm (C4-H and C6-H) and 7.74 ppm (C3-H and C7-H), which become sharp again with time (Fig. 12, see ESI, Fig S29†). In this pH range, the complex reacts to give the double and triple deprotonated species: a fast deprotonation followed by a relatively slow equilibration between the species may explain the evolution of the signals with time. Reaction profile obtained by principal component analysis is presented on Fig. 13.

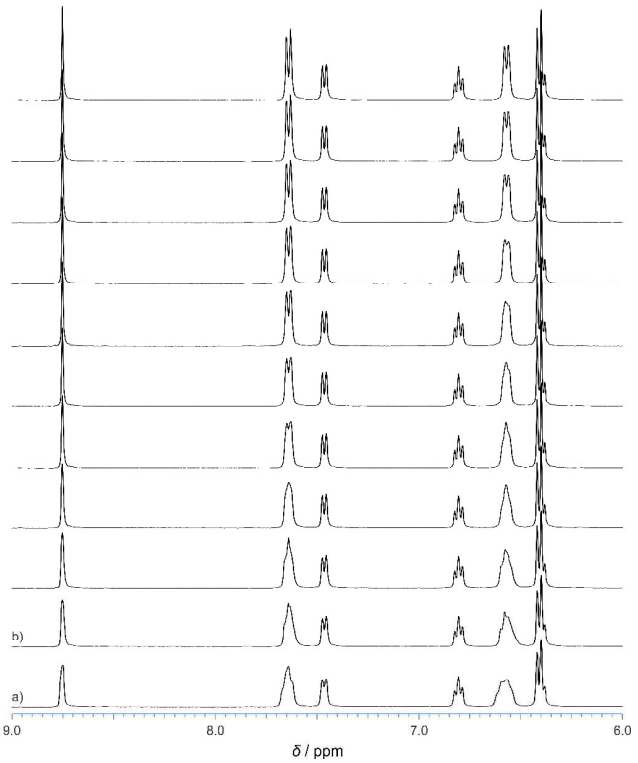

Fig. 12 1H NMR spectrum of complex 1 in DMSO-d_6 (a) with a ratio [NaOH]/ [complex] = 1.1, recorded (a) immediately after the addition; (b) after 15 min. Successive spectra were recorded at intervals of 5 min.

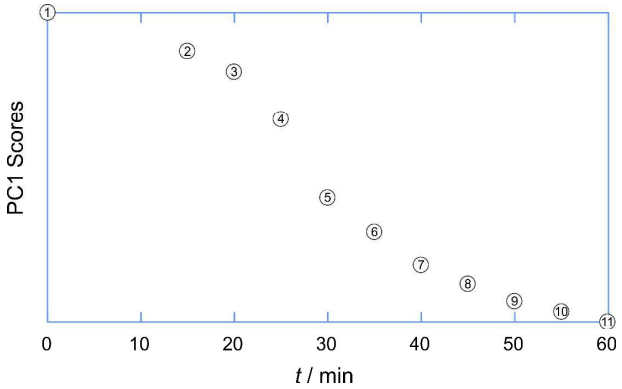

Fig. 13 PC1 scores obtained by principal component analysis of NMR spectra presented on Fig. 12 in dependence of time.

IR spectroscopy

The spectra of all complexes show two set of bands in agreement with formulation of complexes **1**−**6** as [Co(HL)(L)], with singly- and doubly-deprotonated ligands (Scheme 3). Assignments are corroborated with high level quantum chemical calculations. The band characteristic for the C=O group at *ca*. 1645 cm^{-1} (seen in the IR spectrum of H_2L) is shifted to 1545−1515 cm^{-1} in the spectra of the complexes, suggesting coordination of hydrazonato HL^- ligand through the carbonyl oxygen atom. On the other hand, the presence of a new band in the range of 1385–1280 cm^{-1}, due to stretching vibrations of the C−O bond, suggests

View Article Online
DOI: 10.1039/C5RA22068H

tautomerism (=N−NH−(C=O)− ⇆ =N−N=(C−OH)−), deprotonation and coordination of hydrazidato L^{2-} form through the oxygen atom.

In the IR spectra of the ligands vibration bands belonging to $C{=}N_{imine}$ and $C{-}O_{phenolic}$ groups are found at *ca*. 1630 and 1355 cm^{-1}, respectively. In the case of HL^- ligand these bands are shifted to 1614−1606 cm^{-1} and 1386−1380 cm^{-1}. For L^{2-} ligand they are found at lower wavenumbers (in the range 1607–1598 cm^{-1} and 1285–1241 cm^{-1}). This finding clearly indicates coordination of the ligands to the metal centre through the nitrogen and oxygen atoms of these two groups.

UV-Vis spectroscopy

The electronic absorption spectrum of the ligands H_2L^1 and H_2L^4 exhibit several absorption bands with distinct maxima at 290, 300 and 328 nm and at 289, 300 and 329 nm, respectively. These transitions are assigned to the intra-ligand charge transfer transitions.[58,59] Similar results are observed for H_2L^2 and H_2L^5 (at 303, 312 and 342 nm and at 303, 311 and 341 nm, respectively) as well as for H_2L^3 and H_2L^6 (at 291, 302 and 331 nm and at 292, 302 and 332 nm, respectively).

The cobalt(III) complexes display absorptions with maxima at 402 and 421 nm (**1**), 400 and 421 nm (**2**), 392 and 413 nm (**3**), 405 and 423 nm (**4**), 410 and 429 nm (**5**), and at 398 and 416 nm (**6**). These transitions correspond to the ligand-to-metal charge transfer transitons.[60] Each complex displays additional bands in the higher energy region characteristic for intra-ligand transitions.

Conclusions

The work presented here demonstrates the mechanochemical strategy as a successful route for the preparation of the aroylhydrazone ligands. We have indicated the importance of catalytic amounts of methanol/acetanhydride for their synthesis *via* liquid assisted grinding procedure. Desolvation of hydrates and polymorph inter-conversion of the hydrazones result in the formation of the unsolvated forms, three of which have been structurally characterized *via* single crystal X-ray diffraction method.

The mononuclear complexes [Co(HL)(L)] containing differently deprotonated aroylhydrazone ligands have been obtained by the reaction of the corresponding ligand H_2L and $[Co(acac)_3]$ under solvothermal conditions. The molecular and crystal structures analyses of **1**, **2** and **6·MeOH** revealed octahedral arrangement of the tridentate ONO ligands *via* formation of two condensed chelate rings and the presence of both forms of the particular ligand (HL^- and L^{2-}) in the same complex molecule. The bond distances values in the coordination sphere of Co(III) are influenced by many factors such as charge, degree of the ligand deprotonation and involvement of the donor atom into hydrogen bond formation. The stabilization of the particular ligand form in the complex molecules occurs *via* intermolecular hydrogen bond formation between the –NH group of the singly-deprotonated ligand form and the nitrogen atom of the doubly-deprotonated form (in **1**), with the phenolate and methoxy oxygen atoms (in **2**) or with the solvent methanol molecule (in **6·MeOH**). These hydrogen bonds shape different supramolecular assembling modes: 1D infinite chains in **1** and **6·MeOH**, and centrosymmetrical dimers in **2**.

The preferred formation of O–H···O and N–H···N hydrogen bonds in **1** over the O–H···N and N–H···O hydrogen bonds, results in channels that spread in each space dimension of the crystal structure. On the contrary, when formation of O–H···N and N–H···O in **2** is more stable than O–H···O and N–H···N, than the reaction favours the formation of interconnected structure with channels that spread only in one direction. Such channels that are formed in the structure of **2** are suitable for the accommodation of the methanol molecules.

Experimental section

Preparative part. All starting materials, reagents, and metal salt were purchased from commercial sources and used as received. The starting complex $[Co(C_5H_7O_2)_3]$ ($C_5H_7O_2$ = acetylacetonate) was prepared as described in the literature.[61]

Mechanochemical synthesis of H_2L^{1-6}

All reactions were carried out using a Retsch MM200 ball mill operating at 25 Hz frequency. 4-Hydroxybenzhydrazide or benzhydrazide (1 mmol), and the appropriate aldehyde (1 mmol of salicylaldehyde, 3-methoxy-salicylaldehyde or 4-methoxysalicylaldehyde), methanol (40 μL) and acetanydride (5 μL) were placed with two 7 mm grinding balls in a 10 mL stainless steel jar. The reactants were ground for 40 min to obtain H_2L^1, 20 min to obtain $H_2L^2{\cdot}H_2O$, 60 min to obtain $H_2L^3{\cdot}H_2O$, 30 min to obtain H_2L^4, 30 min to obtain $H_2L^5{\cdot}H_2O$ and 60 min to obtain $H_2L^6{\cdot}H_2O$. Then, the samples were left in air at room temperature.

Solvothermal synthesis of cobalt(III) complexes

A mixture of $[Co(C_5H_7O_2)_3]$ (0.42 mmol) and the appropriate aroylhydrazone (0.84 mmol) in methanol (25 mL) was suspended in a 35 mL Teflon liner, which was sealed in an autoclave and heated at 110 °C for 5 h. The solution was allowed to cool slowly, resulting in the formation of dark red almost black product. The obtained product was filtered and dried up to constant weight.

$[Co(HL^1)(L^1)]$ (1). Yield: 0.23 g, 84%. Calc. for $C_{28}H_{21}CoN_4O_6$ (568.422): C, 59.2; H, 3.7; N, 9.9. Found: C, 58.9; H, 3.8; N, 9.7%. TG: calc. Co_3O_4 14.1%, found 14.0%. Selected IR data (cm^{-1}): 1609 ($C{=}N_{HL}$), 1600 ($C{=}N_L$), 1590 (ring C=C), 1545 ($C{=}O_{HL}$), 1389 ($C{-}N_{HL}$), 1380 ($C{-}O_{phenolate,HL}$), 1278 ($C{-}O_L$), 1241 ($C{-}O_{phenolate,L}$). UV-Vis(dmso): λ/nm: 274, 302, 338, 402 and 421. ^{1}H NMR (400 MHz, DMSO-d_6, TMS): δ = 6.54 (t, 1H; C13-*H*), 6.60 (m, 1H**;** C11-*H* **),** 6.75 (d, 2H; C4-*H* and C6-*H*), 6.94 (t, 1H; C12-*H*), 7.59 (d, 1H; C14-*H*), 7.74 (d, 2H; C3-*H* and C7-*H*), 8.89 (s, 1H; C8-*H*), 10.21 (br s, 1H; C5-O*H*).

$[Co(HL^2)(L^2)]$ (2). 0.22 g, 85%. Crystals of the compound **2·0.7MeOH** lose solvated molecules at room temperature and were analyzed as unsolvated species. Calc. for $C_{30}H_{25}CoN_4O_8$ (628.474): C, 57.3; H, 4.0; N, 8.9. Found: C, 57.7; H, 4.3; N, 8.5%. TG: calc. Co_3O_4 12.8%, found 13.1%. Selected IR data (cm^{-1}): 1608 ($C{=}N_{HL}$), 1607 ($C{=}N_L$), 1592 (ring C=C), 1530

View Article Online
DOI: 10.1039/C5RA22068H

($C{=}O_{HL}$), 1392 ($C{-}N_{HL}$), 1384 ($C{-}O_{phenolate,HL}$), 1281 ($C{-}O_L$), 1242 ($C{-}O_{phenolate,L}$). UV-Vis(dmso): λ/nm: 275, 302, 339, 400 and 421. ^{1}H NMR (400 MHz, DMSO-d_6, TMS): δ = 3.61 (s, 3H; OCH_3), 6.16 (m, 2H; C11-*H* and C13-*H*), 6.74 (d, 2H; C4-*H* and C6-*H*), 7.49 (d, 1H; C14-*H*), 7.73 (d, 2H; C3-*H* and C7-H), 8.79 (s, 1H; C8-*H*), 10.23 (br s, 1H; C5-O*H*).

[Co(HL^3)(L^3)] (3). Yield: 0.21 g, 81%. Calc. for $C_{30}H_{25}CoN_4O_8$ (628.474): C, 57.3; H, 4.0; N, 8.9. Found: C, 57.7; H, 4.3; N, 8.5%. TG: calc. Co_3O_4 12.8%, found 13.2%. Selected IR data (cm^{-1}): 1614 ($C{=}N_{HL}$), 1606 ($C{=}N_L$), 1588 (ring C=C), 1536 ($C{=}O_{HL}$), 1388 ($C{-}N_{HL}$), 1384 ($C{-}O_{phenolate,HL}$), 1286 ($C{-}O_L$), 1241 ($C{-}O_{phenolate,L}$). UV-Vis(dmso): λ/nm: 274, 339, 392 and 413. ^{1}H NMR (400 MHz, DMSO-d_6, TMS): δ = 3.36 (s, 3H; OCH_3), 6.42 (t, 1H; C13-*H*), 6.54 (d, 1H; C12-*H*), 6.72 (d, 2H; C4-*H* and C6-*H*), 7.21 (d, 1H; C14-*H*), 7.72 (d, 2H; C3-*H* and C7-*H*), 8.88 (s, 1H; C8-*H*), 10.18 (br s, 1H; C5-O*H*).

[Co(HL^4)(L^4)] (4). Yield: 0.18 g, 82%. Calc. for $C_{28}H_{23}CoN_4O_4$ (536.424): C, 62.7; H, 3.9; N, 10.4. Found: C, 62.3; H, 3.8; N, 10.25%. TG: calc. Co_3O_4 15.00%, found 14.65%. Selected IR data (cm^{-1}): 1606 ($C{=}N_{HL}$), 1598 ($C{=}N_L$), 1593 (ring C=C), 1519 ($C{=}O_{HL}$), 1389 ($C{-}N_{HL}$), 1386 ($C{-}O_{phenolate,HL}$), 1283 ($C{-}O_L$), 1282 ($C{-}O_{phenolate,L}$). UV-Vis(dmso): λ/nm: 270, 300, 336, 405 and 423. ^{1}H NMR (400 MHz, DMSO-d_6, TMS): δ = 6.49 (t, 1H; C13-*H*), 6.53 (d, 1H**;** C_{11}-*H* **)**, 6.89 (t, 1H; C12-*H*), 7.36 (d, 2H; C4-*H* and C6-*H*), 7.45 (m, 1H; C5-*H*), 7.57 (d, 1H; C14-*H*), 7.87 (d, 2H; C3-*H* and C7-*H*), 8.91 (s, 1H; C8-*H*).

[Co(HL^5)(L^5)] (5). Yield: 0.18 g, 73%. Calc. for $C_{30}H_{25}CoN_4O_6$ (598.491): C, 60.4; H, 4.2; N, 9.4. Found: C, 59.9; H, 3.4; N, 9.1%. TG: calc. Co_3O_4 13.5%, found 13.8%. Selected IR data (cm^{-1}): 1606 ($C{=}N_{HL}$), 1599 ($C{=}N_L$), 1592 (ring C=C), 1514 ($C{=}O_{HL}$), 1391 ($C{-}N_{HL}$), 1384 ($C{-}O_{phenolate,HL}$), 1285 ($C{-}O_L$), 1282 ($C{-}O_{phenolate,L}$). UV-Vis(dmso): λ/nm: 269, 305, 339, 410 and 429. ^{1}H NMR (400 MHz, DMSO-d_6, TMS): δ = 3.63 (s, 3H; OCH_3), 6.17 (s, 1H; C11-*H*), 6.20 (d, 1H; C13-*H*), 7.39 (m, 2H; C4-*H* and C6-*H*), 7.48 (m, 2H; C5-*H* and C14-*H*), 7.86 (d, 2H; C3-*H* and C7-*H*), 8.86 (s, 1H; C8-*H*).

[Co(HL^6)(L^6)] (6·MeOH). Yield: 0.18 g, 71%. Calc. for $C_{31}H_{29}CoN_4O_7$ (598.491): C, 59.05; H, 4.95; N, 8.9. Found: C, 59.2; H, 4.7; N, 8.7%. TG: calc. for MeOH 5.1%, found 5.2%; TG: calc. Co_3O_4 12.8%, found 13.0%. Selected IR data (cm^{-1}): 1606 ($C{=}N_{HL}$), 1598 ($C{=}N_L$), 1591 (ring C=C), 1514 ($C{=}O_{HL}$), 1389 ($C{-}N_{HL}$), 1384 ($C{-}O_{phenolate,HL}$), 1295 ($C{-}O_L$), 1261 ($C{-}O_{phenolate,L}$). UV-Vis(dmso): λ/nm: 267, 342, 398 and 416. ^{1}H NMR (400 MHz, DMSO-d_6, TMS): δ = 3.38 (s, 3H; OCH_3), 6.45 (t, 1H; C13-*H*), 6.56 (d, 1H; C12-*H*), 7.25 (d, 1H; C14-*H*), 7.38 (d, 2H; C4-*H* and C6-*H*), 7.48 (m, 1H; C5-*H*), 7.87 (d, 2H; C3-*H* and C7-*H*), 8.97 (s, 1H; C8-*H*).

Physical methods

Elemental analyses were provided by the Analytical Services Laboratory of the Ruđer Bošković Institute, Zagreb. Thermogravimetric (TG) analysis was carried out with a Mettler-Toledo TGA/SDTA851e thermobalance using aluminum crucibles. All experiments were recorded in a dynamic atmosphere with a flow rate of 200 cm^3 min^{-1}. Heating rates of 5 K min^{-1} were used for all investigations. Differential scanning calorimetry (DSC) measurements were carried out with a Mettler-Toledo DSC823e calorimeter and analyzed by the Mettler STAR^e 9.01. software. Fourier Transform Infrared spectra (FT-IR) were recorded in KBr pellets with a Perkin-Elmer 502 spectrophotometer. Spectra were recorded in the spectral range between 4500−450 cm^{-1}. 1D and 2D ^{1}H NMR spectra were recorded on a Jeol EX-400 instrument (^{1}H at 400 MHz and ^{13}C at 100.4 MHz). Electronic absorption spectra were recorded at 25 °C on a Cary 100 UV-Vis Spectrophotometer.

X-Ray Crystallography. Powder diffraction.

The powder X-ray diffraction data were collected by the Panalytical X'Change powder diffractometer in the Bragg-Brentano geometry using CuK_α radiation. The sample was contained on a Si sample holder. Patterns were collected in the range of $2\theta = 5 - 50°$ with the step size of 0.03° and at 1.5 s per step. The data were collected and visualized using the X'Pert programs Suite.[62]

X-Ray Crystallography. Single crystal diffraction.

The SCXRD data collection for all three ligands and complex **6·MeOH** were conducted with an Oxford Xcalibur diffractometer equipped with 4-circle kappa geometry and CCD Sapphire 3 detector graphite–monocromated MoKα radiation (λ = 0.71073 Å) at 296(2) K using ω-scans. Single-crystal X-ray diffraction data collection for structures **1** and **2** was performed on Oxford Xcalibur Gemini diffractometer equipped with Sapphire CCD detector and graphite–monocromated CuKα radiation (λ = 1.5418 Å) at 296(2) K using ω-scans. The data for complex **2** has been later collected again with the Oxford Xcalibur diffractometer at 150(2) K in order to verify the presence of residual density which has been interpreted as the solvent voids capable to fit certain amount of MeOH molecule.

Data collection for all structures has been performed by applying the CrysAlis Software system.[63] The Lorentz-polarization effect was corrected and the intensity data reduced and the empirical absorption correction (by the multi-scanning method) were performed, all with the CrysAlis software package.[63] The diffraction data have been scaled for absorption effects by the multi-scanning method. Structures solutions were accomplished by using direct methods followed by differential Fourier syntheses. Structure refinement was performed on F^2 by weighted full-matrix least-squares. Programs SHELXS-2013[64] and SHELXL-2013[64] integrated in the WinGX[65] software system (Version 2013.3) were used to solve and refine structures. All non-hydrogen atoms were refined anisotropically. Hydrogen atoms not involved in hydrogen bonding were placed in geometrically

View Article Online
DOI: 10.1039/C5RA22068H

idealized positions and they were constrained to ride on their parent atoms [Csp^2−-H 0.93 Å with U_{iso}(H) = 1.2 U_{eq}(C) and Csp^3-H 0.96 Å with U_{iso}(H) = 1.5 U_{eq}(C)], while the others are found as a peaks of small electron-densities in difference electron-density Fourier maps and refined with the restrained O-H (0.82 Å) and N−H (0.86 Å) distances and assigned isotropic displacement parameters being 1.2 times larger than the equivalent isotropic displacement parameters of the parent atoms.

As the compound H_2L^6 crystallizes in non-centrosymmetric space groups (*Pc*) due to the absence of significant anomalous scattering, the absolute structure could not be determined reliably and the corresponding Flack parameter was omitted from the final cif file (Flack parameter refined to a value of 0.8(10)).

In the complex **2·0.7CH$_3$OH** the refinement of occupancy factors for the O1 and C1 methanol atoms gave value of 0.7. Due to that, the performance of data collection at 150(2) K is undertaken in order to confirm the presence of residual density in the crystal voids and it is also interpreted, but more reliably, as the 0.7 MeOH molecule per complex molecule. The final refinement procedure has been performed by PLATON SQUEEZE instruction at 296(2) K data.

The complex **6·MeOH** contains disordered MeOH molecule with two possible spatial orientation of MeOH molecule within unit cell. This is imposed by the crystallographically determined setting of the carbon C16 atom at the 2-fold rotation axis. Therefore, the occupancy factors of the carbon C16 and oxygen O4 atom have been refined necessarily as fixed value of 0.5. The assignment of the type of atom has been performed on the basis of the type of disorder as well as by participation of the oxygen O4 atom in the hydrogen bonds formation with proton-donor groups of complex molecule (N2-H12N, C7-H7 and C8-H8; see ESI Table S3a). No hydrogen atoms have been assigned to the atoms of MeOH molecule.

The molecular geometry calculations were performed by PLATON (Version 130614)[66] and PARST programs[67] integrated in the WinGX software system. Drawings were made using Mercury[68] and POV-Ray[69]. Selected crystallographic and refinement data for structures obtained *via* single-crystal X-ray diffraction are summarized in Tables 4 and 5. Main geometrical features (selected bond distances and angles) along with hydrogen bond geometry for the structures are given in Table S1−S3, respectively.

Table 4. Crystal data and structure refinement for ligands H_2L^3, H_2L^5 and H_2L^6

Ligand	H_2L^3	H_2L^5	H_2L^6
Chemical formula	$C_{15}H_{14}N_2O_4$	$C_{15}H_{14}N_2O_3$	$C_{15}H_{14}N_2O_3$
M_r	286.28	270.28	270.28
Crystal system, color and habit	monoclinic, colourless, block	monoclinic, pale yellow, prism	monoclinic, colourless, prism
Crystal dimensions (mm^3)	0.21 x 0.31 x 0.45	0.08 x 0.18 x 0.36	0.11 x 0.19 x 0.38
Space group	$P2_1/c$(No. 14)	$P2_1/n$(No. 14)	Pc(No. 7)
Z	4	4	4
Unit cell parameters:			
a /Å	15.1547(3)	9.1617(5)	11.4472(6)
b /Å	8.3437(2)	6.1414(4)	12.6502(9)
c /Å	10.9630(2)	23.4795(12)	9.4907(5)
α/°	90	90	90
β/°	101.307(2)	94.806(5)	97.657(5)
γ/°	90	90	90
V /Å^3	1359.33(5)	1316.45(13)	1362.09(14)
D_{calc} /g cm^{-3}	1.399	1.364	1.318
μ /mm^{-1}	0.103	0.097	0.093
F(000)	600	568	568
Index range	*h:* –19 to 20, *k:* –11 to 11, *l*: –14 to 14	*h:*–11 to 9, *k:* –7 to 7, *l*: –22 to 29	*h:*–14 to 14, *k:* –16 to 16, *l*: –11 to 12
Reflections collected	18347	8242	15072
Independent reflections	3447 [$R_{(int)}$ = 0.019]	2848 [$R_{(int)}$ = 0.027]	5950 [$R_{(int)}$ = 0.055]
Number of reflections with [I>2σ(I)]	2778	1832	3419
Data / restraints / parameters	3447/ 3/200	2848 / 2 / 188	5950/ 6 / 375
Final R^a indices [I>2σ(I)]	R_1 = 0.0402; wR_2 = 0.1044	R_1 = 0.0458; wR_2 = 0.0940	R_1 = 0.0644; wR_2 = 0.1456
R^b indices (all data)	R_1 = 0.0514; wR_2 = 0.1122	R_1 = 0.0862; wR_2 = 0.1078	R_1 = 0.1190; wR_2 = 0.1735

[a] $R = \Sigma||F_o| - |F_c||/ \Sigma|F_o|$; [b] $wR = \{\Sigma[w(F_o^2 - F_c^2)^2]/\Sigma[w(F_o^2)^2]\}^{1/2}$

View Article Online
DOI: 10.1039/C5RA22068H

Table 5. Crystal data and structure refinement for complexes **1**, **2** and **6**·**MeOH**

Complex	**1**	**2**	**6**·MeOH
Chemical formula	$C_{28}H_{21}CoN_4O_6$	$C_{30}H_{25}CoN_4O_8$	$C_{30}H_{25}CoN_4O_6 \cdot CH_3OH$
M_r	568.42	628.47	624.48
Crystal system, color and habit	Orthorhombic, dark red plate	Triclinic, dark red, irregular beaked plate	Monoclinic, dark red cube block
Crystal dimensions (mm^3)	0.22 × 0.19 × 0.07	0.51 × 0.29 × 0.17	0.63 × 0.49 × 0.47
Space group	*I b c a* (No. 73)	$P\ \bar{1}$(No. 2)	*C* 2/*c* (No.15)
Z	8	2	4
Unit cell parameters:			
a /Å	11.5874(6)	10.2428(4)	21.903(4)
b /Å	18.9530(9)	12.2495(4)	10.2910(8)
c /Å	23.1420(14)	13.1323(6)	12.5225(8)
α/°	90	102.594(3)	90
β/°	90	107.080(4)	98.436(10)
γ/°	90	97.463(3)	90
V /Å^3	5082.4(5)	1503.55(11)	2792.0(5)
D_{calc} /g cm^{-3}	1.486	1.388	1.486
μ /mm^{-1}	5.737	4.953	0.672
F(000)	2336	648	1288
Index range	*h:* –7 to 14, *k:* –20 to 23, *l*: –27 to 28	*h:* –12 to 12, *k*: –14 to 14, *l*: –15 to 15	*h*: –27 to 27, *k*: –13 to 13, *l*: –15 to 14
Reflections collected	8906	14096	7034
Independent reflections	2410 [$R_{(int)}$ = 0.0785]	5693[$R_{(int)}$ = 0.0465]	2915[$R_{(int)}$ = 0.0313]
Number of reflections with [$I>2\sigma(I)$]	1742	4808	2383
Completeness to θ= 67.68° (25.24° for **6**·MeOH)	100.0 %	99.9 %	96.0%
Data / restraints / parameters	2410 / 2 / 183	5693 / 3 / 399	2915/2/204
Final R^a indices [$I>2\sigma(I)$]	R_1 = 0.0512; wR_2 = 0.1151	R_1 = 0.0530; wR_2 = 0.1485	R_1 = 0.0502; wR_2 = 0.1184
R^b indices (all data)	R_1 = 0.0736;wR_2 = 0.1305	R_1 = 0.0628;wR_2 = 0.1568	R_1 = 0.0635; wR_2 = 0.1248

[a] $R = \Sigma||F_o| - |F_c||/\ \Sigma|F_o|$; [b] $wR = \{\Sigma[w(F_o^2 - F_c^2)^2]/\Sigma[w(F_o^2)^2]\}^{1/2}$

Computational Methods

Geometry optimizations for the unit cells were performed using the hybrid functional using B3LYP hybrid functional and D3 version of Grimme's dispersion with Becke-Johnson damping[70] with 6-31g(d) basis set in combination with the 6-31G(d) basis set starting from crystallographically determined structures. Additionally, to quantitatively determine the standard Gibbs energies of binding, harmonic vibrational frequencies were calculated. All quantum chemical calculations were carried out using the Gaussian 09 program package.[71]

Acknowledgments

Financial support for this research was provided by Ministry of Science and Technology of the Republic of Croatia. We acknowledge Edislav Lekšić, PhD, for X-ray single-crystal diffraction data collection for compounds **1** and **2**.

Notes and references

[a] *University of Zagreb, Faculty of Science, Department of Chemistry, Horvatovac, 102a, 10000 Zagreb, Croatia, Fax: ++ 385-1-4606341; Tel: ++385-1-4606353; E-mail: visnja.vrdoljak@chem.pmf.hr*
[b] *University of Zagreb, Faculty of Textile Technology, Division of Applied Chemistry, Prilaz baruna Filipovića 28a, 10000 Zagreb, Croatia.*
[c] *Department of Chemical and Pharmaceutical Sciences, University of Trieste, Via L. Giorgieri 1, 34127, Trieste, Italy*

† Electronic Supplementary Information (ESI) available: (1) DSC thermograms, (2) PXRD patterns, (3) TG curves, (4) figures for compounds (6) Tables of selected bond distances and angles and of hydrogen bonds parameters and (7) ^{1}H NMR spectra. Crystallographic data sets for the structures H_2L^3, H_2L^5, H_2L_6, **1**, **2**, **2**·**0.7MeOH** and **6**·**MeOH** are available through the Cambridge Structural Data base with deposition numbers 1432533-1432539. See DOI: 10.1039/b000000x/

1 M. Hidai and Y. Mizobe, *Chem. Rev*., 1995, **95**, 1115.
2 R. Lazny and A. Nodzewska, *Chem. Rev*., 2010, **110**, 1386.
3 S. Kobayashi, Y. Mori, J. S. Fossey and M. M. Salter, *Chem. Rev.,* 2011, **111**, 2626.
4 P. Vicini, F. Zani, P. Cozzini and I. Doytchinova, *Eur. J. Med. Chem*., 2002, **37**, 553.
5 C. Loncle, J. M. Brunel, N. Vidal, M. Dherbomez and Y. Letourneux, *Eur. J. Med. Chem*., 2004, **39**, 1067.
6 L. Savini, L. Chiasserini, V. Travagli, C. Pellerano, E. Novellino, S. Cosentino and M. Pisano, *Eur. J. Med. Chem*., 2004, **39**, 113.
7 J.-M. Lehn, *Chem. Soc. Rev*., 2007, **36**, 151.
8 J.-M. Lehn, *Angew. Chem., Int. Ed.,* 2013, **52**, 2836.
9 F. J. Uribe-Romo, C. J. Doonan, H. Furukawa, K. Oisaki and O. M. Yaghi, *J. Am. Chem. Soc.*, 2011, **133**, 11478.
10 D. N. Bunck and W. R. Dichtel, *J. Am. Chem. Soc.,* 2013, **135**, 14952.
11 V. Vrdoljak, B. Prugovečki, D. Matković-Čalogović, R. Dreos, P. Siega and C. Tavagnacco, *Cryst. Growth Des*., 2010, **10**, 1373.
12 Vrdoljak, B. Prugovečki, D. Matković-Čalogović, J. Pisk, R. Dreos and P. Siega, *Cryst. Growth Des*., 2011, **11**, 1244.
13 J.-M. Lehn, *Chem.-Eur. J.*, 2006, **12**, 5910.
14 S. M. Landge and I. Aprahamian, *J. Am. Chem. Soc*., 2009, **131**, 18269.

View Article Online
DOI: 10.1039/C5RA22068H

15 S. M. Landge, E. Tkatchouk, D. Benitez, D. A. Lanfranchi, M. Elhabiri, W. A. Goddard and I. Aprahamian, *J. Am. Chem. Soc*., 2011, **133**, 9812.
16 D. Ray, J. T. Foy, R. P. Hughes and I. Aprahamian, *Nat. Chem.*, 2012, **4**, 757.
17 X. Su, T. F. Robbins and I. Aprahamian, *Angew. Chem., Int. Ed*., 2011, **50**, 1841.
18 S. Rowan, S. Cantrill, G. Cousins, J. Sanders and J. Stoddart, *Angew. Chem., Int. Ed*., 2002, **41**, 898.
19 P. T. Corbett, J. Leclaire, L. Vial, K. R. West, J.-L.Wietor, J. K. M. Sanders and S. Otto, *Chem. Rev.,* 2006, **106**, 3652.
20 Y. Jin, C. Yu, R. J. Denman and W. Zhang, *Chem. Soc. Rev*., 2013, **42**, 6634.
21 R. Raue, A. Brack and K. Lange, *Angew. Chem., Int. Ed. Engl*., 1991, **30**, 1643.
22 R. Lygaitis, V. Getautis and J. V. Grazulevicius, *Chem. Soc. Rev*., 2008, **37**, 770.
23 M. Hong, H.-D. Yin and D.-Q. Wang, *Acta Cryst. E,* 2006, **62**, m1504.
24 N. Mohd Lair, H.Mohd Ali and S. W. Ng, *Acta Cryst. E*, 2009, **65**, m541.
25 N. Mohd Lair, H. Khaledi, H. Mohd Ali and R. Puteh *Acta Cryst. E*, 2010, **66**, m470.
26 H. Yin, *Acta Crystallogr., Sect.C: Cryst. Struct. Commun*., 2008, **64**, m324.
27 L.-F. Zou, X.-Y. Yang, D.-X. Wang, Y. Gao, Y. Wang and Y.-H. Li, *Asian J. Chem*., 2012, **24**, 2909.
28 P. Krishnamoorthy, P. Sathyadevi, P. T. Muthiah and N. Dharmaraj, *RSC Advances*, 2012*,* **2**, 12190.
29 S. Naskar, S. Naskar, S. Mondal, P. K. Majhi, M. G. B. Drew, S. K. Chattopadhyay, *Inorg. Chim Acta*, 2011, **371**, 100.
30 P. V. Bernhardt, J. Mattsson, and D. R. Richardson, *Inorg. Chem*., 2006, **45**, 752.
31 C. M. Armstrong, P. V. Bernhardt, P. Chin and D. R. Richardson, *Eur. J. Chem.* 2003, 1145.
32 S. Taktak, W. Ye, A. M. Herrera and E. V. Rybak-Akimova, *Inorg. Chem.*, 2007, **46**, 2929.
33 M. Haga, M. Ali, S. Koseki, K. Fujimoto, A. Yoshimura, K. Nozaki, T. Ohno, K. Nakajima and D. Stufkens, *Inorg. Chem*., 1996, **35**, 3335;
34 S. Klein, W. G. Dougherty, W. S. Kassel, T. J. Dudley and J. J. Paul, *Inorg. Chem*., 2011, **50**, 2754.
35 Q.-J. Wu and S.-X. Liu, *Jiegou Huaxue (Chin. J. Struct. Chem.)* 2004*,* **23**, 1177.
36 Y.-T. Chen, J.-M. Dou, D.-C.Li, D.-Q. Wang and Y.-H. Zhu, *Acta Crystallogr., Sect. .E : Struct. Rep. Online,* 2007, **63**, m3129.
37 Q.-J. Wu, X.-H. Chen, J. Jiang, B-Q. Cai and Y.-P. Xie *Acta Crystallogr., Sect. E: Struct. Rep. Online,* 2011*,* **67**, m293.
38 G-M. Yu, X.-Y. Yang, Y. Wang, Y.-J. Xiao and Y.-H. Li, *Acta Crystallogr., Sect. E: Struct. Rep. Online,* 2011, **67**, m329.
39 P.-S. Zhao, J. Song, X.-J. Sun, L. Du and F.-F. Jian, *Jiegou Huaxue (Chin. J. Struct. Chem.),* 2011, **30**, 346.
40 D. Matoga, J. Szklarzewicz, K Stadnicka and M. S. Shongwe, *Inorg. Chem.*, 2007, **46**, 9042.. **2007**, 46, 9042-9044
41 H. H. Monfared, S. Sadighian, M.-A. Kamyabi and P. Mayer, *J. Mol. Catal. A: Chemical*, 2009, **304**, 139.
42 S. L. James, C. J. Adams, C. Bolm, D. Braga, P. Collier, T. Friščić, F. Grepioni, K. D. M. Harris, G. Hyett, W. Jones, A. Krebs, J. Mack, L. Maini, A. G. Orpen, I. P. Parkin, W. C. Shearouse, J. W. Steed and D. C. Waddell, *Chem. Soc. Rev*., 2012, **41**, 413.
43 T. Friščić, *Chem. Soc. Rev*., 2012, **41**, 3493
44 G.-W. Wang, *Chem. Soc. Rev*., 2013, **42**, 7668.
45 G. Kaupp, J. Schmeyers and J. Boy, *J. Prakt. Chem*., 2000, **342**, 269.
46 G. Kaupp and J. Schmeyers, *J. Phys. Org. Chem*., 2000, **13**, 388.
47 P. F. M. Oliviera, M. Baron, A. Chamayou, C. André-Barrès, B. Giidetti and M. Baltas, *RSC Advances*, 2014, **4**, 56736.
48 X.-C. Lin, H. Yin and Y. Lin, *Acta Cryst. E*, 2007, **63**, o2864 (CSD code YIFPAF01).
49 J.-F. Lu, *Acta Cryst. E*, 2008, **64**, o2032 (CSD code ROGFEZ).
50 N. Md. Lair, H. Md. Ali and S. W. Ng, *Acta Cryst. E*, 2009, **65**, o189 (CSD code MOKRUA).
51 A. Lyubchova, A. Cosse-Barbi, J. P. Doucet, F. Robert, J.-P. Souron and M. Quarton, *Acta Cryst. C*, 1995, **51**, 1893 (CSD code ZAYQAR).
52 O. Pouralimardan, A.-C. Chamayou, C. Janiak and H. Hosseini-Monfared, *Inorg. Chim. Acta*, 2007, **360**, 1599 (CSD code TEZMER)
53 R. Chan-Navarro, V. M. Jimenez-Perez, B. M. Munoz-Flores, H. V. Rasika Dias, I. Moggio, E. Arias, G. Ramos-Ortiz, R. Santillan, C. Garcia, M. E. Ochoa, M. Yousufuddin and N. Waksman, *Dyes Pigm.*, 2013*,* **99**, 1036 (CSD code MIQXUH).
54 The structure of the H_2L^3 ligand was determined in 2012 [H. H. Rassem, A. Salhin, B. Bin Salleh, M. M. Rosli, H.-K. Fun, *Acta Crystallogr.* 2012, E**68**,o2279], based on the data collected at low temperature (100 K). As most of this study, especially when referring to ligands, was conducted at room temperature we decided to undertake a new structure determination with the data collected at room temperature.
55 A. Blagus, D. Cinčić, T. Friščić, B. Kaitner, V. Stilinović, *Maced. J. Chem. Chem. Eng*., 2010, **29**, 117.
56 S. Grimme, S. Ehrlich and L. Goerigk, *J. Comp. Chem.*, 2011, **32**, 1456.
57 V. Vrdoljak, J. Pisk, D. Agustin, P. Novak, J. Parlov Vuković and D. Matković-Čalogović, *New J. Chem*., 2014, **38**, 6176.
58 K. Chichak, U. Jacquenard and N.R. Branda, Eur. J. Inorg. Chem. 2002, 357.
59 P. Krishnamoorthy, P. Satyadevi, P. T. Mutiah and N. Dharmaraj, *RSC Advances*, 2012, **2**, 12190.
60 T. Ghosh, B. Mondal, T. Gosh, M. Sutradhar, G. Mukherjee and M. G. B. Drew, *Inorg. Chim Acta*, 2007, **360**, 1753.
61 B. E. Bryant and W. C. Fernelius, *Inorg. Synth.*, 1957, **5**, 188.
62 *X'Pert Software Suite*, Version 1.3e; Panalytical B. V., Almelo, The Netherlands, 2001.
63 Oxford Diffraction Ltd., Xcalibur CCD system, CrysAlis Software system, Versions 1.171.36.28 and 1.171.37.33. Abingdon; Oxfordshire, England, 2008.
64 G. M. Sheldrick, *Acta Crystallogr*. 2008, **A64**, 112.
65 L. J. Farrugia, *J. Appl. Crystallogr*., 2012, **45**, 849.
66 A. L. Spek, *J. Appl. Cryst*. 2003, **36**, 7.
67 (a) M. Nardelli, *Comput. Chem.* 1983, **7**, 95; (b) M. Nardelli, *J. Appl. Cryst.* 1995, **28**, 659.
68 C. F. Macrae, I. J. Bruno, J. A. Chisholm, P. R. Edgington, P. McCabe, E. Pidcock, L. Rodriguez-Monge, R. Taylor, M. Towler, J. Van der Streek and P. A. Wood, *J. Appl. Crystallogr*. 2008, **41**, 466.
69 http://www.povray.org/.
70 R. Peverati and D. G. Truhlar, *Phys. Chem. Chem. Phys.*, 2012, **14**, 16187.
71 Gaussian 09, Revision D.01, M. J. Frisch, G. W. Trucks, H. B. Schlegel, G. E. Scuseria, M. A. Robb, J. R. Cheeseman, G. Scalmani, V. Barone, B. Mennucci, G. A. Petersson, H. Nakatsuji, M. Caricato, X. Li, H. P. Hratchian, A. F. Izmaylov, J. Bloino, G. Zheng, J. L. Sonnenberg, M. Hada, M. Ehara, K. Toyota, R. Fukuda, J. Hasegawa, M. Ishida, T. Nakajima, Y. Honda, O. Kitao, H. Nakai, T. Vreven, J. A. Montgomery, Jr., J. E. Peralta, F. Ogliaro, M. Bearpark, J. J. Heyd, E. Brothers, K. N. Kudin, V. N. Staroverov, T. Keith, R. Kobayashi, J. Normand, K. Raghavachari, A. Rendell, J. C. Burant, S. S. Iyengar, J. Tomasi, M. Cossi, N. Rega, J. M. Millam, M. Klene, J. E. Knox, J. B. Cross, V. Bakken, C. Adamo, J. Jaramillo, R. Gomperts, R. E. Stratmann, O. Yazyev, A. J. Austin, R. Cammi, C. Pomelli, J. W. Ochterski, R. L. Martin, K. Morokuma, V. G. Zakrzewski, G. A. Voth, P. Salvador, J. J. Dannenberg, S. Dapprich, A. D. Daniels, O. Farkas, J. B. Foresman, J. V. Ortiz, J. Cioslowski, and D. J. Fox, Gaussian, Inc., Wallingford CT, 2013.

View Article Online
DOI: 10.1039/C5RA22068H

Table of contents entry

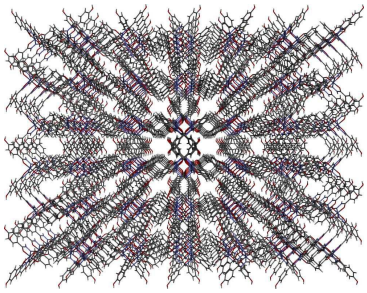

Differently protonated ligands in [Co(HL)(L)] are stabilized *via* supramolecular assembling through O–H···O/N and N–H···N/O hydrogen bonding. Channels spreading either in each space dimension or predominantly in one direction are formed.